



Analysis and validation of a procedure for a lumped model of Polar Class ship shafting systems for transient torsional vibrations

Giorgio Burella¹ · Lorenzo Moro¹ · Dan Oldford²

Received: 29 April 2017 / Accepted: 28 October 2017 / Published online: 27 November 2017
© JASNAOE 2017

Abstract

In this paper, the authors discuss the development of a procedure for modeling the transient torsional loads on shafting systems induced by an ice impact sequence on Polar Class vessels propellers. The procedure was used to solve the transient torsional vibration using a lumped masses model of shafting systems driven by electric motors. After a description of the methodology and procedure used to model the vibratory behavior of a shafting system, the discussion will focus on a sensitivity analysis performed on the relevant parameters that allows a proper description of the shaft's dynamics. The model has then been benchmarked and validated against the results from a finite element code, using an R-Class icebreaker from the Canadian Coast Guard as a case study. The results show promising outcomes for the assessment of the transient torque loads, and the model will be used in the future to aid the upcoming experimental activity.

Keywords Polar Class · Lumped model · Sensitivity analysis · Ice loads · Transient torsional vibration analysis

1 Introduction

Arctic navigation has consistently increased in the last few decades, driven by the exploitation of the unveiled natural resources in the region. Even though the level of investment for this purpose has decreased in the last few years, the exploitation and development of Arctic traffic of vessels will continue [1]. For instance, it is forecast that more and more passenger ships will undertake polar routes, especially in exploring cruises [2], leading to increased safety concerns for Arctic-going vessels as more people traverse ice-infested routes.

It is anticipated that more ships will be assigned to or constructed for such services and there is an increased need for reliable and sustainable ship design procedures. This has led to research efforts towards proper assessment of the ship–ice interaction that is inevitable in that environment. The design inputs have to include the ice loads expected over the life-time of the vessel. These loads, among others, affects important systems such as the propulsion machinery. The loss of this system can produce severe hazard for the safety of navigation, and jeopardize the survival of the crew and passengers. In recent years, there has been much study on the ice loads acting on the propulsion system. The thrust and bending moment acting on the blades during the interaction of the propeller with the water and ice can be divided in three components: a separable hydrodynamic load (open water condition), an inseparable hydrodynamic load (increased torque and thrust due to blockage) and ice milling/impact loads [3]. Several experiments have been carried out to measure the loads induced by the propeller–ice interaction in an ice towing tank [4–9]. Numerical procedures have been developed to predict the hydrodynamic loads due to blockage [10], ice contact loads [11] or both [12].

The knowledge gained in ice loading on the propulsion system eventually led to the proposal of a design approach for the whole shafting system [13]. The International Association of Classification Societies (IACS) has been

✉ Giorgio Burella
gburella@mun.ca

Lorenzo Moro
lmoro@mun.ca

Dan Oldford
doldford@eagle.org

¹ Ocean and Naval Architectural Engineering, Memorial University of Newfoundland, 240 Prince Phillip Drive, St. John's, NL A1B3X5, Canada

² Harsh Environment Technology Center, American Bureau of Shipping (ABS), 240 Prince Phillip Drive, St. John's, NL A1B3X5, Canada

developing a set of harmonized rules for polar vessels that includes requirements for the propulsive machinery [14]. These rules have been also adopted by the American Bureau of Shipping (ABS), introducing requirements for vessels intended for Polar Class notation [15]. For the shafting systems in particular, it is required to assess the maximum torque responses during the dynamic response to a milling sequence or subsequent ice impacts. The load pattern is provided by the rules according to the specific ship's Polar Class and characteristic.

Shaft torsional vibrations and dynamic responses have long been known and studied. The peak and hazardous response of all the systems in the propulsive machinery subjected to the ice impacts is transient. In recent times, several studies focused on the development of models and procedures for a proper assessment of transient torsional vibration analysis (TTVA) to assess the maximum torque loads in the shafting [16, 17]. The response of the machinery system as a whole depends on the behavior and interaction of the subsystems, as shown in Fig. 1, the mass-elastic behavior of the shaft, the presence of torsional dampers, clutches, gears, the type of propeller, the type of prime mover, and the speed-control system [18]. All the aforementioned papers expose and analyze methodologies to assess TTVA under prescribed ice loading conditions. Both Batrak et al. [16] and Barro and Lee [17] make use of a lumped-parameter model to simulate the shaft dynamics, while Polic et al. [18] introduce also an alternative modal-parameter model of the shaft, using the bond-graph method. The models presented by Batrak et al. [16] and Polic et al. [18] also take into account the dynamics of diesel engines with a speed controller. Polic et al. [18] present an extensive analysis of the sensitivity of the bond-graph model to the system parameters. These studies have provided insights into the modeling of the dynamics of Polar Class ship shafting systems. Nevertheless, the

state-of-the-art literature review shows that any variation of the load scenarios as a function of the Polar Class and their effect on the shafting system's dynamic response have not yet been investigated. Furthermore, a guidance on the minimum number of lumps to properly model the dynamic transient behavior of a flexible shaft has not been provided.

This paper presents the recent outcomes of ongoing research between Memorial University of Newfoundland and the Harsh Environment Technology Center (HETC) of ABS on the development of a procedure for assessing the TTVA of Polar Class shafting systems. Here, we focused on modeling of the mass-elastic properties of a shafting system as a system of lumps, rather than the other relevant subsystems.

The authors present the results of a sensitivity analysis on a general two-lumps shaft, aiming to give guidance for the minimum number of lumps to describe the transient dynamics of a generally shaped flexible shaft. Later, we consider a shafting system from an R-Class icebreaker and we present the transient torque response using the same procedure applied to the developed lumped-mass model and a finite-element model. The loads are varied for all the load cases considered in the Polar Class rules. Influence of the main simulation parameters is considered on this simulation. Finally, we discuss and compare the results for the two models of the case study in order to get useful indications for future work and proper modeling.

2 Methods

The task of modeling the torsional vibration and the torque response in the shaft of a Polar Class ship requires the thorough description of each subsystem of the propulsive machinery. When a diesel engine is considered, the model requires a high level of detail. This means that transient engine characteristics such as the air intake, turbocharger, combustion, injection, governor and reciprocating mass are required to be included in the model [19]. Also, the existence of a z-drive propulsion unit calls for modeling the presence of gearboxes. In the following work, the authors concentrated on the proper modeling of the shaft behavior not considering the influence of speed control systems on the shaft response.

For this reason focus was put on a procedure to model a generally gear-branched shafting system driven by an electric motor. Thus, for the current application of the methodology, the presence of the speed controller was not modeled, assuming that the synchronous motor is delivering a constant power. The delivered torque was modeled accordingly, and adding a torque cap $Q_{mot,0}$ for low motor speeds, as shown in Fig. 2, in such a way, in the transient simulation, the speed drop due to the ice impact is eventually modeled.

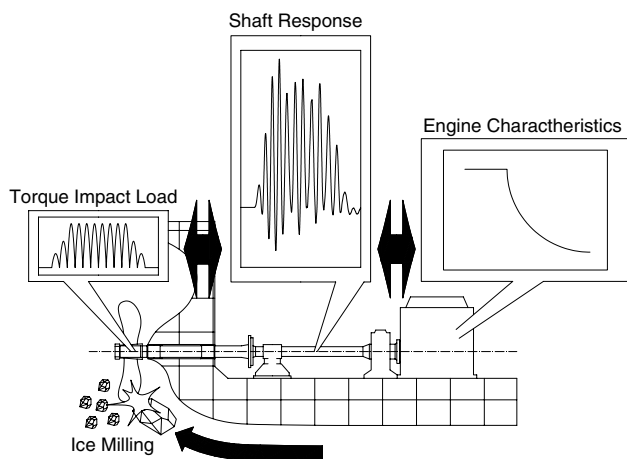


Fig. 1 The response of the shaft, depending on the behavior of the single propulsive machinery subsystems

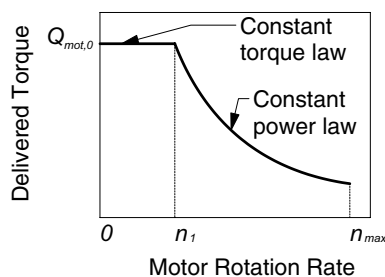


Fig. 2 Electric motor-delivered torque characteristic

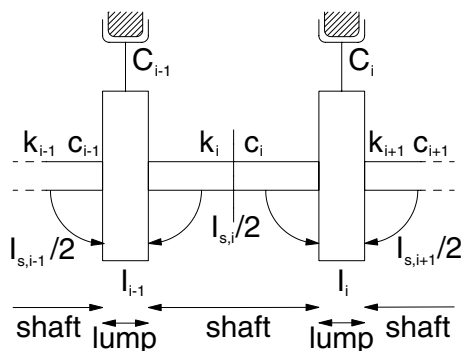


Fig. 3 Lumped masses model of a portion of the shaft: k is the shaft equivalent stiffness, c the relative damping, I_s the moment of inertia of the shaft, I the moment of inertia of relevant lumps at nodes and C the absolute damping

2.1 Lumped parameters model

The dynamics of a flexible shaft was modeled using the classic approach of a linear lumped masses system [20]. In this approach, the mass is lumped at the shaft ends and at locations where relevant rotary masses are present (flywheels, bearing disks, gears). These locations, called nodes, are assigned with a polar moment of inertia I and a degree of freedom (DOF). The latter is the rotation about their axis $\theta(t)$, a function of time. The mass of the shaft is included in the lumps, split in half between adjacent nodes, as shown in Fig. 3.

The torsional elastic behavior of the shaft is modeled using classical beam theory to obtain an equivalent torsional stiffness k from node to node. The presence of tapers, steps and hollow sections in the shaft between node is accounted for using the concept of series of equivalent torsional stiffness [21].

Linear viscous damping torque proportional to the relative velocity between adjacent nodes is used to model the damping of the material, called relative damping [16]. The latter is assumed to be proportional to the shaft equivalent stiffness. Hence the relative damping coefficient for the generic shaft element (i , shaft) can be written as:

$$c_{i,shaft} = \frac{\kappa k_{i,shaft}}{\omega}, \tag{1}$$

where ω is a rotation phase velocity and $k_{i,shaft}$ is the torsional equivalent stiffness of the considered shaft element. The coefficient κ is a damping ratio for the shaft material representative of the ratio of damping torque to the elastic response torque. Viscous damping can be also applied directly to the rotating lumps and is called absolute damping.

The dynamics are represented via the classic equation of motion:

$$[I] \ddot{\theta}(t) + [C] \dot{\theta}(t) + [K] \theta(t) = \mathbf{Q}(t), \tag{2}$$

where $[I]$ is an inertia matrix, $[C]$ is a damping matrix. $[K]$ is a singular stiffness matrix, $\mathbf{Q}(t)$ is a load vector of external torques applied at nodes and $\theta(t)$ is the nodal rotation vector. The matrices are assembled using a finite element procedure for gear-branched shafting systems [22].

2.2 Loads treatment

The external loads are the hydrodynamic open water torque, the impact torque acting on the propeller(s) and the delivered torque by the motor(s), applied at their respective nodes.

The hydrodynamic load of the propeller is modeled with a simple power law, depending on the rotation rate of the node. The propeller during the ice milling sequence is operating in an unsteady state. The adsorbed torque curve is steeper than the open water one. The exponent for the propeller power law is taken such as the adsorbed torque is function of power higher than 2 of the propeller rotation rate, according to the Archer number A [23, 24]. Assuming that more than one propeller can be present in the shafting system, the adsorbed torque law for the node (p, i) is then written as:

$$Q_{hydro}(\dot{\theta}_{p,i}(t)) = c_{Q_0} \dot{\theta}_{p,i}^a(t), \tag{3}$$

where the constant c_{Q_0} depends on the propeller open water characteristics, and a is an exponent that is taken to be bigger than 2. Archer’s Number A is calculated by $A = 9.55a$. $A \approx 20$ for most of the conventional propellers in steady-state operation.

The impact torque is provided by the Polar Class rules from ABS [15], and is a function of the angular position at the propeller node, implicitly depending on time. The torque loading is given by a sequence of half-sine impacts given by the following function:

$$Q_{imp}(\theta_{p,i}(t)) = C_q Q_{max} \sin\left(\theta_{p,i}(t) \frac{180}{\alpha_i}\right). \tag{4}$$

Depending on the Polar Class (7–1) and the impact cases (1–3), the coefficients C_q , α_i and the maximum impact torque Q_{max} are given, as well as the number of impacts in

the propeller–ice interaction sequence. Both ice impact and hydrodynamic loads are summed and applied to the propeller loads can then be summed up in a unique torque load at the generic propeller at node (p, i) the torque load can be defined as:

$$Q_{\text{prop},(p,i)}(t) = -Q_{\text{imp}}(\theta_{p,i}(t)) - Q_{\text{hydro}}(\dot{\theta}_{p,i}(t)). \quad (5)$$

As outlined before, assuming that the model can present more than one motor, the delivered torque from the electric motor at the generic node (e, j) with spin velocity $\theta_{e,j}(t)$ is modeled according to a constant delivered power law. For lower speeds, a torque cap $Q_{\text{eng},0}$ for the delivered torque is introduced. The delivered engine torque as function of the rotation rate is then expressed via the following definition:

$$Q_{\text{mot},(e,j)}(\dot{\theta}_{e,j}(t)) = \begin{cases} Q_{\text{mot},0} & 0 \leq \dot{\theta}_{e,j} \leq n_1 \\ \frac{P_{\text{mot}}}{\dot{\theta}_{e,j}(t)} & n_1 \leq \dot{\theta}_{e,j} \leq n_{\text{max}}, \end{cases} \quad (6)$$

where the speed range from $0 \leq \dot{\theta} \leq n_1$ presents a constant delivered torque behavior and the range $n_1 < \dot{\theta} \leq n_{\text{max}}$ presents constant delivered power behavior. n_1, n_{max} represents limit rotation rate for the motor delivered torque behavior. P_{mot} is the delivered power from the engine, that as mentioned before, is considered constant and set to the value of interest (i.e., rated power). The data regarding the torque motor characteristics are usually provided by the motor's manufacturer. The torque law described in Eq. 6 is shown in Fig. 2.

2.3 Time solution

The solution for the set of n ($=$ number of nodes) second-order ordinary equations is done solving a state space formulation. The latter is a set of $2n$ first-order ordinary differential equations [25], that can easily be solved with any implicit or explicit time integration algorithm. In this case, an explicit Runge–Kutta algorithm implemented in *MATLAB*® is used to solve the differential equations.

The initial condition for the time solution are set so that the system nodes are spinning at the set rated speed and the system is twisted due to the steady-state torque load over the shaft.

At each time step, the load level at the motor and propeller nodes is updated taking into account the current level of displacement and velocity. Since the loads, following Sect. 2.2, implicitly depend on time, at each time step the loads are interpolated from the defining functions that depend on the nodes' displacements and velocities at the start of the time step.

Once the solution is obtained, the displacement and velocity at the nodes are processed to obtain the torque

response. This is due to the reactive forces of the torsional stiffness and relative damping between two adjacent nodes. Once the response is calculated, the maximum (Q_{peak}) and minimum (Q_{min}) peak torques can be obtained from the time series and the torque amplitude, for each shaft component is obtained as:

$$Q_A = |Q_{\text{peak}} - Q_{\text{min}}|. \quad (7)$$

3 Finite element model

In this research activity, the need of a benchmark case to compare the results of the lumped model with, led the authors to develop equivalent finite element models of the shaft system considered. A commercial finite element code (*ANSYS*®) was used to develop the structural models, using two approaches for the structural shaft components:

1. Structural solid modeling, using structural brick 3D elements.
2. Structural 3D linear beam elements modeling, given that the slenderness of a beam is high enough.

The element size in both cases was tuned so that enough divisions were present in the length span of the shaft to capture properly the first 10 torsional modes. For the solid models, only regular mapped meshing is used, so that nodes in the longitudinal span are lying in the cross sections.

The lumps were modeled with point masses provided with mass and moments of inertia equivalent to the actual mass distribution of the corresponding lump. The structural damping can be modeled according to these two approaches [26]:

1. Using Rayleigh damping, and setting the damping matrix proportional to the stiffness

$$[C]_{\text{FEM}} = \frac{\kappa}{\omega} [K]_{\text{FEM}}. \quad (8)$$

2. Using a constant critical damping ratio ζ , if the solution to response in both frequency and time domain are obtained using modal superposition.

The loads for the time domain solution, likewise the lumped model in Sect. 2.2, are interpolated from their definition using the levels of the degrees of freedom at the end of the previous time-step. The torque moment response is calculated in the post-processing phase. In a cross section of the shaft, the nodes are selected. The contribution of the structural elements connected on one side is then summed. In this manner, the total torque moment acting on one cross section side is obtained, for each time-step. For internal balance this moment is equal to the one on the other side.

4 Sensitivity analysis

Once the methodology was set and the procedure verified using the available literature, the authors performed a sensitivity analysis for the model. A two degrees of freedom (2-DOFs) shaft with point masses at both extremities was modeled. The authors believe that this example was meaningful, since it is the minimum representation of a marine shafting system, usually consisting of a propeller and a motor that can be represented as point masses at the opposite extremities of a shaft. This model, as shown in Fig. 4 is described through the moments of inertia from point masses at the end nodes I_1 and I_2 , that are connected via a cylindrical shaft of length L and diameter D , respectively. The material properties were selected in the general case of a steel shaft, i.e., $E_{steel} = 210$ GPa and $\rho_{steel} = 7850$ kg/m². The inertia of the shaft I_{shaft} , the damping and equivalent torsional stiffness of the shaft can be obtained from first principle formulas.

The aim of this analysis is to investigate the minimum requirement on the parameters sets to properly assess the dynamics of the system. The lumped model created following this paper’s procedure is benchmarked against an equivalent finite element model developed in ANSYS® for the same basic shafting system. The latter is modeled using solid brick elements for the shaft, and two point masses representing the

point masses at the ends, with equivalent mass properties of a thin cylindrical flywheel.

The criteria used to compare the models are the following:

1. Match of the system’s undamped natural frequencies
2. Match of the frequency response function for the torque response
3. Match of the transient response to a single ice impact

4.1 Parameters variation matrix

Four main dimensional parameters were identified: I_1 , I_2 , I_{shaft} , L , D . Three dimensionless parameters were used for variation in the analysis: I_1/I_2 , I_1/I_{shaft} , L/D . The parameters outlined are varied as detailed in Table 1.

The finite element models created in this sensitivity analysis present three degrees of freedom for each node, due to the use of solid bricks to model the flexible shaft between

Table 1 Variation of the nondimensional parameters for the sensitivity analysis of the 2-DOFs system

Parameter	Values
I_1/I_2	1, 5, 10, 15, 20
I_1/I_{shaft}	0.1, 0.5, 1, 2, 5, 10, 20, 40, 60
L/D	2, 5, 10, 15, 20, 25

Fig. 4 Outline of a generic lumped 2-DOFs shafting model for the torsional vibrations and modeling using commercial finite element

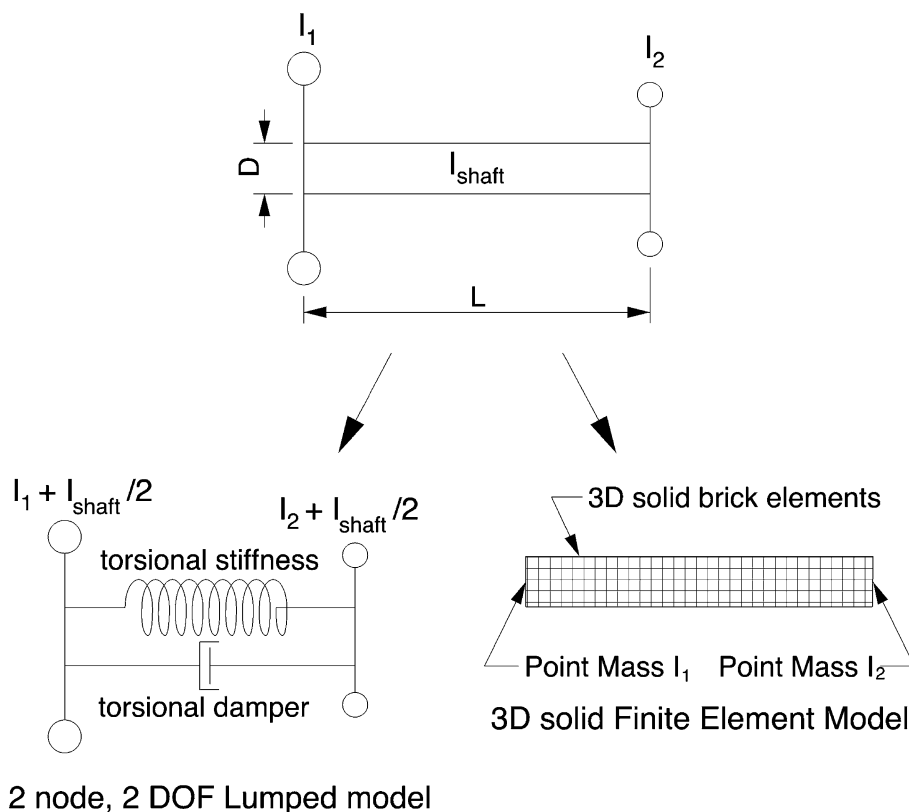


Table 2 Percentage difference (%) in natural frequency between lumped and finite element model, 1st torsional mode, $I_1/I_{\text{shaft}} = 2$

L/D	I_1/I_2				
	1	5	10	15	20
2	5.41	2.63	2.22	2.08	2.01
5	5.42	2.64	2.23	2.09	2.02
10	5.42	2.65	2.24	2.10	2.03
15	5.42	2.65	2.24	2.10	2.03
20	5.42	2.65	2.24	2.10	2.03
25	5.42	2.65	2.24	2.10	2.03

Table 3 Percentage difference (%) in natural frequency between lumped and finite element model, 1st torsional mode, $I_1/I_{\text{shaft}} = 1$

L/D	I_1/I_2				
	1	5	10	15	20
2	10.36	5.65	4.82	4.53	4.38
5	10.37	5.66	4.83	4.54	4.39
10	10.37	5.67	4.83	4.54	4.40
15	10.37	5.67	4.84	4.54	4.40
20	10.37	5.67	4.84	4.54	4.40
25	10.37	5.67	4.84	4.54	4.40

two lumps. Thus, a modal analysis will produce not only the torsional modes, but also, for instance, the bending modes of the shaft. The lumped model of the same has only two nodes with one degree of freedom (i.e., the rotation about their axis) and thus 2-DOFs only. The dynamics of such an unconstrained 2-DOF system is fully described by only two natural modes, a rigid motion with zero frequency and a torsional mode. For this reason, a comparison is provided only for the first torsional mode.

4.2 Results of the sensitivity analysis

The outcome shows important results for proper modeling a shaft. It is often reported in literature that the assumption of lumped masses is consistent as long as its moment of inertia is small compared to the adjacent point masses inertias. In this sensitivity analysis it was found that, given a threshold of 5% on the percentage difference of the natural frequencies, it is consistent to model the shafting with lumped masses when $I_1/I_{\text{shaft}} \geq 2$, as seen in Table 2. Above the latter threshold, the ratio of the moments of inertia I_1/I_2 and the shaft slenderness ratio L/D does not affect the difference, but just the magnitude of each natural frequency when the parameters are varied.

Below $I_1/I_{\text{shaft}} \leq 2$, as shown in Table 3 the modeling can still be good, given that the ratio $I_1/I_2 \geq 10$. This result is particularly useful in a shaft that presents two adjacent

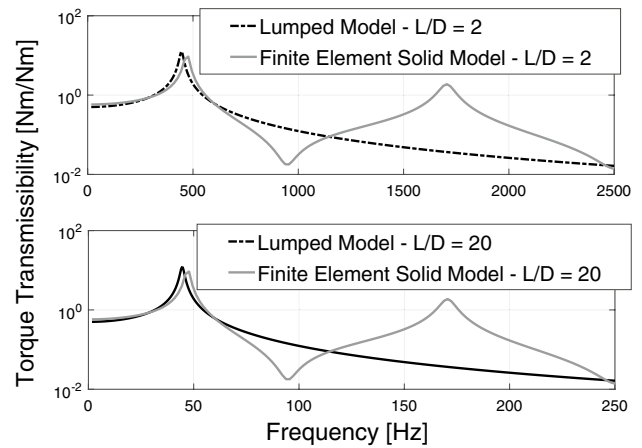


Fig. 5 Frequency response function for the torque response of the shaft, $\zeta = 0.02$, for node 1, force applied at node 1, $I_1/I_{\text{shaft}} = 2$, $I_1/I_2 = 1$, $L/D = 2, 20$

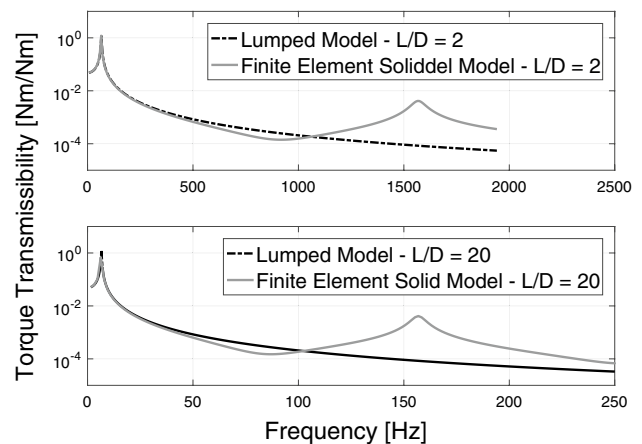


Fig. 6 Frequency response function for the torque response of the shaft, $\zeta = 0.02$, for node 1, force applied at node 1, $I_1/I_{\text{shaft}} = 60$, $I_1/I_2 = 20$, $L/D = 2, 20$

lumps at the ends, one lumped mass several times heavier than the other, the lumped assumption is still valid if the lightest lump has moment of inertia comparable to the one of the shaft.

The response torque in the shaft of an applied torque at node 1 was studied as well. In Figs. 5 and 6 the amplitudes of the frequency response functions (FRFs) for the aforementioned quantity are presented. The behavior of this function to the parameters L/D , I_1/I_{shaft} and I_1/I_2 can be synthesized in the statements:

1. The second torsional mode has peak amplitude comparable to the one from the first torsional mode when the mass of the shaft is comparable to the lumps ($I_1/I_{\text{shaft}} = 2$) and I_1/I_2 is close to unity.

- The influence of the slenderness L/D is not affecting the shape and the amplitude of the peaks, but is shifting the peaks in the frequency. Higher L/D will mean lower natural frequencies and consequently peaks positioned in the lower frequencies band.

The influence of the presence of appreciable response from higher torsional mode on the transient damped response was inspected. In this case, the system with $L/D = 20$, $I_1/I_{\text{shaft}} = 2$, $I_1/I_2 = 1$ was selected, in order to have low natural frequencies and second torsional (and higher) mode response comparable to the one from the first. Its transient response to a single half-sine impact applied to node 1 was calculated, using two different impulses with impact time span $\Delta\tau_{\text{imp}} = 0.001 - 0.01\text{s}$. The first was used to excite a large range of frequencies and modes, while the second was used to excite mainly the first torsional mode. The response was calculated for both the lumped and finite element model, the latter presenting the modes higher than the first torsional. In Figs. 7 and 8, the comparison of the two models is presented for both $\Delta\tau_{\text{imp}}$. The behavior of the simulated curves is quite different when the higher modes are included in the response. Appreciable differences are seen in the maximum and minimum peaks of the transient response (Fig. 7). Hence when modeling an n-DOFs lumped model, it is important to include and properly model at least the presence of the first few higher modes, and to check the presence of appreciable higher torsional modes in the frequency response functions. A time lag on the free vibration after the impact is found due to the difference on first torsional mode for the two models (around 5).

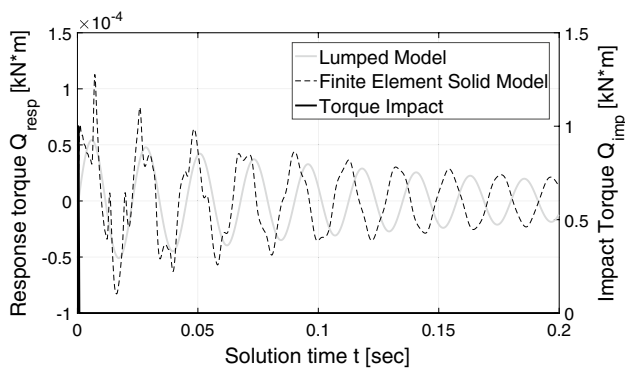


Fig. 7 Torque response on the shaft for a half-sine impulse applied at node 1, $\Delta\tau_{\text{imp}} = 0.001\text{s}$, $\zeta = 0.02$

5 Case study: R-Class icebreaker

With the knowledge on modeling built up during the sensitivity analysis, the authors selected a case study. This was identified in an existing R-Class ice breaker from the Canadian Coast Guard, and the preliminary results of this analysis were presented in [27]. This vessel was built in the 1980s, and have proven to be a reliable and robust design for the Arctic navigation. The propulsive system is driven by an AC synchronous electric motor (Table 4). The outline is shown in Fig. 9.

A solid cross-section steel shaft is connecting the prime mover to the propeller hub. The coupling to the motor is direct, with no torsional damper or elastic coupling. The shaft is arranged in three sections, from the propeller to the aft bearing of the motor: a tailshaft extending for a portion in the machinery space, an intermediate shaft and the motor shaft. The tailshaft is supported by sea-water lubricated bearings in the sterntube. No bearing is present between the forward sterntube bearing and the motor thrust bearing. The tailshaft and intermediate shaft are linked with a tapered fit coupling. On the aft section of the terminal flange a brake disk is installed. The intermediate shaft is coupled via a

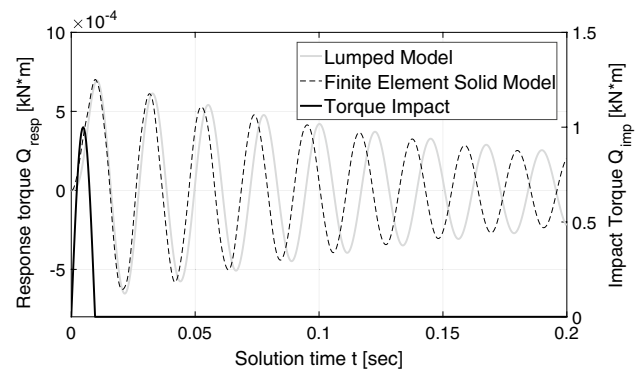


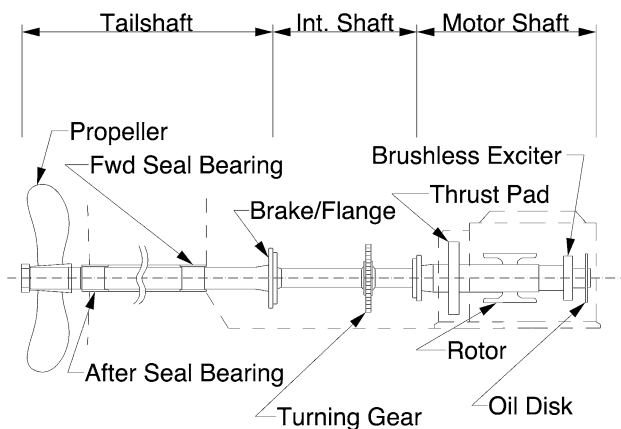
Fig. 8 Torque response on the shaft for a half-sine impulse applied at node 1, $\Delta\tau_{\text{imp}} = 0.01\text{s}$, $\zeta = 0.02$

Table 4 Main dimensions and characteristics of the R-Class ice breaker

Symbol	Quantity	Value
L_{OA}	Length overall (m)	99.8
Z	Number of blades	4
D_{prop}	Propeller diameter (m)	4.12
d_{prop}	Bossing diameter (m)	1.1151
$P_{0.7R}$	Propeller pitch (m)	3.3045
P_{mot}	Rated motor delivered power (MW)	6
n_{mot}	Rated motor speed (rpm)	180

Table 5 Mass-elastic data from the shafting system

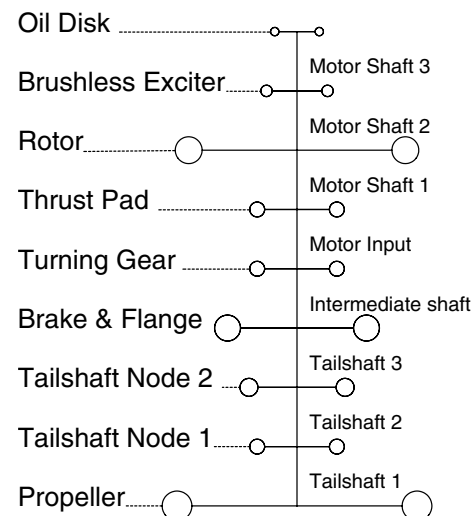
Node name	Lumped moments of inertia (kg m^2)	
Propeller	16499	
Tailshaft node 1	477	
Tailshaft node 2	738	
Brake and flange	1008	
Turning gear	207	
Thrust Pad	316	
Rotor	10634	
Brushless exciter	99	
Oil disk	15	
Shaft element	Stiffness ($\frac{\text{MN}}{\text{rad}}$)	Rel. Damp. ($\frac{\text{Nm s}}{\text{rad}}$)
Tailshaft 1	64.030	33478
Tailshaft 2	271.325	14187
Tailshaft 3	319.346	16697
Intermediate shaft	221.177	11565
Motor input	700.821	36643
Motor shaft 1	329.330	17219
Motor shaft 2	323.500	16915
Motor shaft 3	279.471	14613

**Fig. 9** Outline of the case study shafting

flange to the motor shaft, on which a turning gear is present. The engine shaft has a thrust collar, a rotor, brushless exciter and a forward bearing.

Relevant lumps are identified in the following list (Fig. 10):

1. Propeller and entrained water
2. Tailshaft/intermediate shaft flange and brake
3. Turning gear
4. Thrust bearing collar and pads
5. Rotor
6. Brushless exciter

**Fig. 10** R-class shafting system lumped model with names of lumps and shaft sections

7. Oil disk/forward motor bearing.

5.1 Mass-elastic system

In order to evaluate the lumped model parameters, some assumptions are made. The shaft couplings are assumed to be stiff enough to be modeled as rigid connections and no flange or taper fit connection stiffness is considered. The relevant lump locations are used for placing the model's nodes.

Since the tailshaft section has a high moment of inertia for the shaft so that the ratio $I_{brake}/I_{shaft} \leq 2$, the latter is subdivided in two sections. Hence two additional nodes, at which the mass of the shaft is lumped, are placed between the propeller and the brake disk. Equivalent torsional stiffness is calculated in between nodes, and the mass-elastic data are reported in Table 5.

The damping is calculated according to Eq. 1, using a phase velocity equal to $\omega = 2\pi f_{1st\ tors}$, that corresponds to the lower torsional mode natural frequency. A dimensionless damping ratio $\kappa = 0.005$ was used.

5.2 R-Class loads characteristics

The torque loads are applied to the rotor node (driving torque) and the propeller node (Open water load and ice-impact torque). This also means that a part of the shaft is unloaded. The mapping of the torque motor to the rotation speed is done according to Eq. 6, using the specification from the actual motor. The characteristic is showed in Fig. 11.

The propeller adsorbed torque is modeled according to Eq. 3. The Archer coefficient used to model the exponent of the power curve was set to 20. The characteristic curve of adsorbed torque is presented in Fig. 11.

The impact torque is provided by the Polar Class rules from ABS for each impact case and Polar Class.

5.3 Calculation setup

The aim of the analysis is to compare the transient response of the developed lumped model to the ice impacts with the response of the finite element model. The comparison has been produced for each Polar Class (1–7) and each impact case (1–3) and consisted in calculating the maximum peak

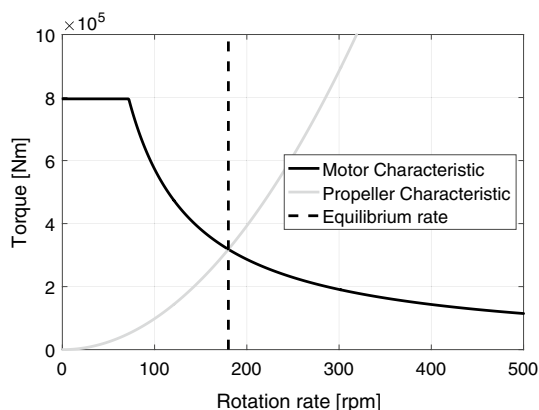


Fig. 11 R-class electric motor constant power delivered torque and propeller open water adsorbed torque

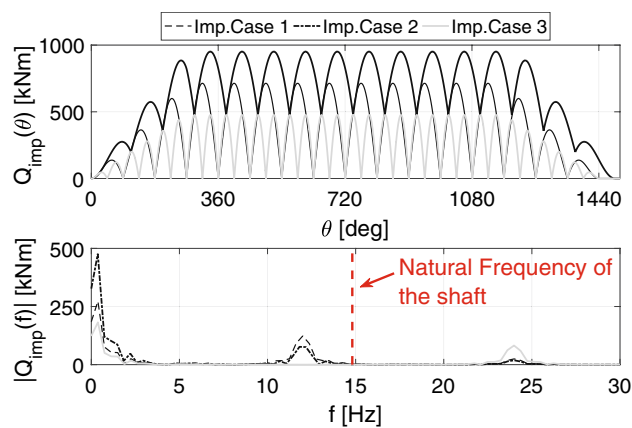


Fig. 12 Polar Class 5 ice impact torque: on top, impact torque definition at propeller position, on bottom, the amplitude of the Fourier transform at constant propeller rotation rate $n_{prop} = 180$ [rpm]

torque in the shaft elements Q_{peak} and the maximum torque amplitude Q_A as defined in the Polar Class rules.

Solid brick and a beam finite element models modal analysis was used to justify the usage of a beam model in the calculation of a transient response. This is because the latter model has slightly lower computational times for the transient response. Proper boundary conditions were placed in order to simulate the bearings in the tailshaft and on the motor shaft.

In order to include the first four torsional modes in the response, the time step of the solution for the finite element model was set to $\Delta t_{calc,FE} = 1/500$ s. A lower time step $\Delta t_{calc,FE} = 1/1200$ s was also used to study the influence of this parameter to the response and hence the inclusion of higher modes. In the lumped model the time step for the transient solution is set to a lower value ($\Delta t_{calc,Lump} = 4.5 \cdot 10^{-4}$ s). This is done for a twofold reason:

1. The solver implemented in *MATLAB*® is explicit, hence requires a little time-step for the stability of the solution
2. Such a little time step includes all the modes predicted by the lumped model.

5.4 Ice impact loads

The shape of the impact torque, depends on the Polar Class and on the impact case. The impact amplitudes ramp up of 270° at the beginning of the sequence and ramp down for 270° at the end. The amplitude of the torque impacts depends on the propeller characteristics, on the Polar Class (higher torques are prescribed for the higher class) and on the impact case (each impact case has a different amplitude magnifier). The number of ice impacts are described thoroughly by the Polar Class (by the size of the ice block) and impact case. For the latter, impact case 1 and 2 consider a

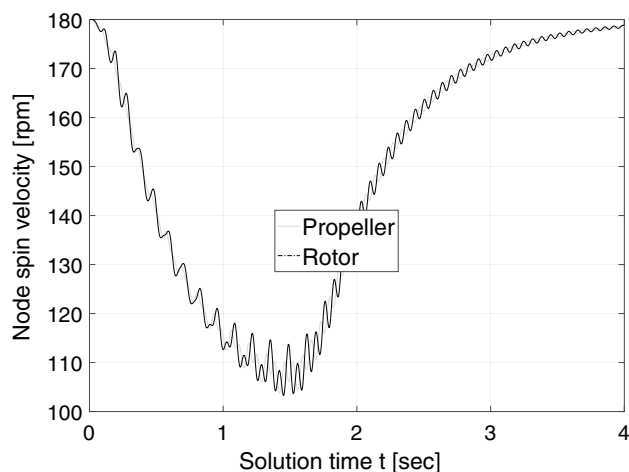


Fig. 13 Speed drop and recovery for PC 5, IC 1. (IC impact case; PC Polar Class)

Table 6 Number of impacts for the case study

PC	IC	No. of imps.	Q_{\max} (kN m)
1	1, 2	32	1110
	3	64	
2	1,2	28	1110
	3	56	
3	1, 2	24	1110
	3	48	
4	1, 2	20	1110
	3	40	
5	1, 2	16	952
	3	32	
6	1, 2	14	610
	3	28	
7	1, 2	12	515
	3	24	

PC Polar Class, IC impact case

single impact per blade passage on the milling of the ice block, while case 3 considers two impacts on one blade per blade passage. For the case study, the number of impacts are reported for each considered condition in Table 6.

If the impacts were to happen at constant rotation rate (as shown in Fig. 12 for Polar Class 5) the most of the energy of the impacts would be concentrated at the blade passage frequency and higher harmonics, as well as the zero frequency, representative of a mean impact torque. For impact case 3 the energy would be concentrate at double the blade passage frequency and higher harmonics, since the impacts are doubled for each blade passage. In reality, due to the speed drop shown in Fig. 13, the peaks will smear and shift to lower frequencies, this effect being

more accentuated the more the speed is dropping (and hence slower impacts).

5.5 Results from the transient analysis

The first results to be presented are the natural frequencies from the modal analysis. The finite element solid and beam model results were compared with the lumped masses for the match of the torsional modes.

In Table 7 it can be seen that the error is minimum for the first torsional mode (in the order of 1%) and increases with the higher modes, but still acceptable up to the third. It was considered consistent to use the finite element beam model to calculate the transient, since it was close to the solid model in the natural frequencies and hence in the description of the model's dynamics. This reduced drastically the computational time when running the finite element code. Calculation times for the beam finite element model at different time steps and the lumped models are shown in Table 8.

Table 9 reports the maximum peak torque Q_{peak} and the torque amplitude Q_A in the transient response as defined by the Polar Class rules. The values presented in the results for Polar Class 1–4, impact case 1 are the same. This is due to the fact that, for the case study considered, the maximum impact torque Q_{max} and the ramp up of the values of the first impacts are the same for the aforementioned Polar Classes (for this particular vessel), even though the overall number of impacts is different. The maximum and minimum peak response torque are placed usually during the ramp up and ramp down of the torque impacts, producing the same values for the aforementioned load cases.

The maximum peak torque and amplitude for the transient response torque of impact case 2 of Polar Class 1–4 are not reported. This is because the delivered motor torque is not able to overcome these impact load scenarios. The shaft is hence decelerating, and eventually stopping. Even after this, the overall loads on the shaft yield to a further deceleration of the shaft, that reverse the spin. A transient response can be calculated, but no clear maximum peak torque or amplitude can be extracted, since the torque response lead a periodical steady-state pattern, as shown in the response time-history in Fig. 14, as the shaft speed fluctuate between forwards and backwards spin velocities. This pointed out an issue with the modeling of impacts that eventually lead to the aforementioned spurious shaft dynamic response. No statement is found on this case in the Polar Class, or about any propulsive power minimum requirements. The ice torque impact law defined in the rules assumes that the impacts are happening in sequence without the propeller stopping or spinning backwards.

This behavior can be expected also for models that include a speed governor, since for electrical motors a torque

Table 7 Torsional modes natural frequencies comparison for R-Class icebreaker

Natural frequencies			
Modes	Lump. Mod.	FEM solid	FEM beam
1	14.81	14.59	14.87
2	64.82	61.11	62.09
3	144.32	136.11	139.01
4	177.20	195.91	198.50
Percentage difference (FEM beam vs lumped model)			
Modes		Lump. Solid	Lump. Beam
1		1%	0%
2		6%	4%
3		6%	4%
4		– 11%	– 12%

Table 8 Computational times for the transient responses

Model	Δt_{calc} (s)	Computational time (s)
Lumped	$\approx \frac{1}{4500}$	$\approx 9\text{E} + 02$
FEM beam element	$\frac{1}{500}$	$\approx 5.4\text{E} + 03$
FEM beam element	$\frac{1}{1200}$	$\approx 1.3\text{E} + 04$

Δt_{calc} is the constant time step for the transient solution

limiter is always present in the speed control algorithms. The maximum deliverable torque can be reached and the ice impact torque can exceed this value as the Polar Class is increased.

The maximum differences in Q_{peak} and Q_A among the whole shaft span were extracted from the torque response time history for each loading case, as shown in Table 10. The maximum peak response torque Q_{peak} shows the best behavior in terms of percentage differences between lumped and finite element models, leading to a maximum difference around 3–4%. Larger differences were found in the results related to Polar Class 6 and 7. As far as Polar Class 7 is concerned, the maximum difference in torque amplitude Q_A is 12%, in the case of $\Delta t = \frac{1}{500}$, and 13% in the case of $\Delta t = \frac{1}{1200}$. The maximum torque amplitude Q_A is found during the ramp down of the impact loads, as seen in Figs. 15 and 16. It is worth pointing out that in these cases higher torsional modes contribute to build up the difference in peak and minimum transient torques. This happens because the speed drop is smaller for Polar Class 6 and 7, when compared to higher Polar Classes, and this implies that the down-shift of the harmonic peaks from the blade passage frequency and harmonics is also smaller. Therefore, higher modes are excited.

In order to understand better the influence of the torsional modes on the total response, we calculated the frequency response function of the system. Figure 17 shows the

mobility response functions calculated at ‘Thrust Pad’ node when a unitary torque is applied at the ‘Propeller Node’. The comparison of the frequency response functions shows that the lumped model properly simulates the first torsional mode of the shaft system. We can also notice the lower mobility in correspondence of the second and third mode of the lumped model, while the two frequency response functions do not match at higher frequencies. This behavior of the mobility functions was observed for each mobility function calculated at each node of the shafting system, and is causing the higher transient response of the lumped model in the peak and minimum reaction torques. The authors think that this is likely due to the Rayleigh-like damping that considers only terms proportional to the stiffness, which are usually responsible for the higher frequencies damping only.

6 Conclusions

A procedure for modeling a lumped model of shafting systems intended for the assessment of torsional ice-impact loads was developed and presented in the paper. The procedure is based on proven literature, and provides a methodology to model the mass-elastic model of the shafting system driven by an electric motor and the loads acting during the transient loading from a sequence of ice-impacts as described by the ABS Polar Class rules.

The relevant parameters affecting the dynamics of the system were studied in a sensitivity analysis on the simplest case of a 2-DOFs lumped model in comparison to an equivalent finite element model. The relevant parameters were the moments of inertia ratios and shaft slenderness. In order to consistently assume lumped masses in a shaft, the optimal moment of inertia ratios were found. The slenderness ratio did not affect the correctness of the assumption, but merely shifted the natural frequencies. The response to a single

Table 9 Tabular results from maximum peak Q_{peak} and amplitude Q_A response torques, for each performed calculation

PC	IC	Lmp. Md. (kNm)		FEM beam e.l.s (kNm)		FEM beam e.l.s (kNm)	
		Q_{peak}	Q_A	$\Delta t_{calc} = \frac{1}{1200} s$		$\Delta t_{calc} = \frac{1}{500} s$	
				Q_{peak}	Q_A	Q_{peak}	Q_A
1	1	1106	1094	1118	1122	1109	1106
	2	–	–	–	–	–	–
	3	1290	1613	1276	1592	1275	1579
2	1	1106	1094	1118	1122	1109	1106
	2	–	–	–	–	–	–
	3	1266	1570	1255	1554	1253	1541
3	1	1106	1094	1118	1122	1109	1106
	2	–	–	–	–	–	–
	3	1202	1454	1198	1448	1195	1436
4	1	1106	1094	1118	1122	1109	1106
	2	–	–	–	–	–	–
	3	1070	1205	1068	1204	1062	1190
5	1	1049	1096	1053	1108	1046	1096
	2	1005	729	999	722	998	720
	3	658	430	660	434	657	430
6	1	676	458	678	459	680	464
	2	788	552	791	559	788	555
	3	461	149	464	163	456	152
7	1	628	400	630	401	631	405
	2	620	350	620	353	618	350
	3	432	123	424	117	425	113

PC Polar Class, IC impact case

Table 10 Tabular results from maximum peak Q_{peak} and amplitude Q_A response torques differences between the lumped and finite element models, for each performed calculation

	$\Delta t_{calc} = \frac{1}{500} s$			$\Delta t_{calc} = \frac{1}{1200} s$		
	IC1 (%)	IC2 (%)	IC3 (%)	IC1 (%)	IC2 (%)	IC3
Percentage difference Q_A (%)						
PC1	– 4	–	– 3	– 3	–	– 2
PC2	– 4	–	– 2	– 3	–	– 2
PC3	– 4	–	– 2	– 3	–	– 1
PC4	– 4	–	– 4	– 3	–	– 2
PC5	– 3	– 5	– 4	– 2	– 5	2
PC6	– 6	– 4	– 5	– 7	– 4	11
PC7	– 6	– 6	– 12	– 7	– 6	– 13
Percentage difference Q_{peak} (%)						
PC1	– 2	–	– 2	– 1	–	– 2
PC2	– 2	–	– 2	– 1	–	– 1
PC3	– 2	–	– 1	– 1	–	– 1
PC4	– 2	–	– 2	– 1	–	– 1
PC5	– 1	– 2	– 2	– 1	– 2	– 1
PC6	– 3	– 1	– 2	– 3	– 1	2
PC7	– 3	– 1	– 2	– 3	– 1	– 2

PC Polar Class, IC impact case

Negative values means that the lumped model values are higher

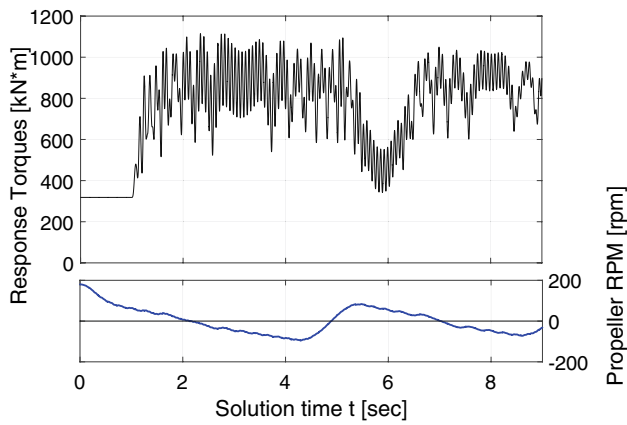


Fig. 14 Transient torque response, ‘Tailshaft 1’ shaft component, for the lumped model, PC4, impact case 2

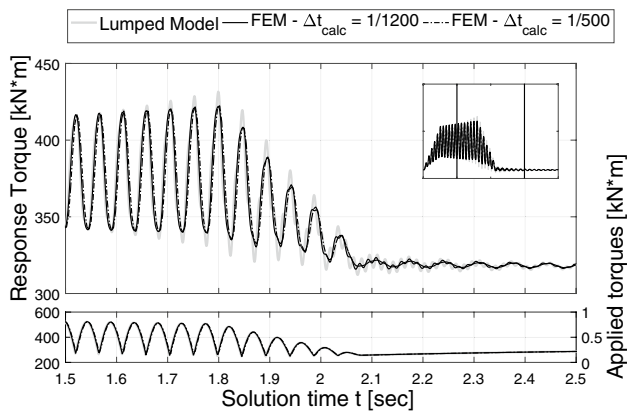


Fig. 15 Transient torque response, ‘Motor Shaft 1’ shaft component, for the lumped model, PC7, impact case 3

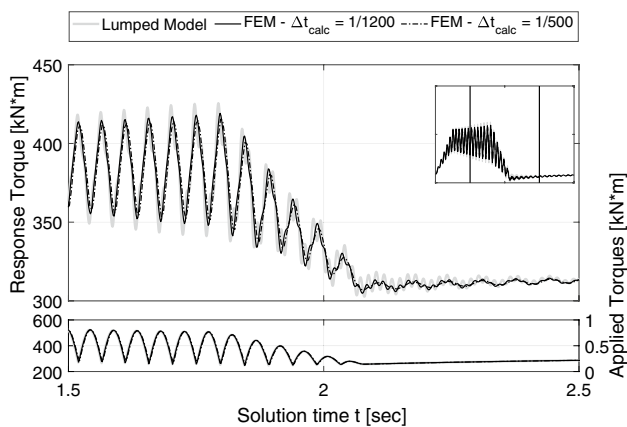


Fig. 16 Transient torque response, ‘Tailshaft 1’ shaft component, for the lumped model, PC7, impact case 3

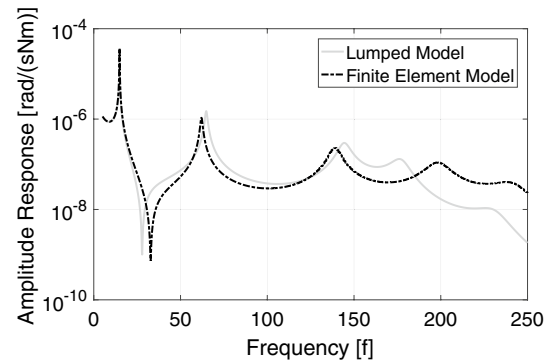


Fig. 17 Frequency response function for the mobility of the ‘Thrust Pad’ Node to a unitary torque applied at the ‘Propeller node’

ice-impact was studied and compared using the lumped and finite element models. This showed that the lower torsional modes have an influence on the differences between highest and lowest transient response torque peaks, which are important to the Polar Class rules. Hence the first few higher modes must be properly modeled.

Then, the authors applied the presented procedure to calculate the transient torque response of the shafting system of an R-Class icebreaker from the Canadian Coast Guard. The results from the simulations were benchmarked against the outcomes of FE dynamic analysis. The models showed good agreement for Polar Class loading cases from 1 to 5, where higher-than-2 torsional modes are not contributing consistently to the whole transient response.

The research activity pointed out several topics to be inspected in future work. Firstly, experiments should be conducted in order to collect data from instrumented shafts on-board icebreakers. This will allow the researchers to understand completely the dynamic response of shafting systems subjected to ice-impacts, and thus improve both knowledge of the modeling of lumped models and loading on the shafts of Polar Class vessels. This will lead to a better understanding of the phenomena related to relative and absolute damping components (such as propeller damping), which was addressed marginally in this work. Another future activity is to extend the modeling procedure to diesel engine applications, including the behavior of speed-governors.

Acknowledgements The authors thank the American Bureau of Shipping (ABS), the Research & Development Corporation of Newfoundland and Labrador (RDC) and Mr. Mike Chaisson from the Canadian Coast Guard for their important and kind contribution to the presented research activity, without which the latter would not have been possible.

References

- Buorne JKJ (2016) In the Arctics cold rush, there are no easy profits. National Geographic, March 2016. <https://www.national-geographic.com/magazine/2016/03/new-arctic-thawing-rapidly-circle-work-oil/>. Accessed 21 Nov 2016
- Stewart EJ, Howell SE, Draper D, Yackel J, Tivy A (2007) Sea ice in Canada's Arctic: implications for cruise tourism. *Arctic* 60(4):370–380
- Wang J, Akinturk A, Bose N (2009) Numerical prediction of propeller performance during propeller-ice interaction. *Mar Technol* 46(3):123–139
- Moores C, Veitch B, Bose N, Jones S, Carlton J (2003) Multi-component blade load measurements on a propeller in ice. *Trans Soc Naval Architects Mar Eng* 110(2003):169–187
- Wang J, Akinturk A, Jones SJ, Bose N, Kim M, Chun H (2007) Ice loads acting on a model podded propeller blade. *J Offshore Mech Arct Eng* 129(3):236–244
- Doucet J, Bose N, Veitch B, Liu P (1997) Experimental results and theoretical predictions of loading on an ice-class ducted propeller. In: 4th Canadian marine hydromechanics dynamics conference, Ottawa, Canada
- Karulina M, Karulin E, Belyashov V, Belov I (2008) Assessment of periodical ice loads acting on screw propeller during its interaction with ice. In: International conference and exhibition on performance of ships and structures in ice, ICETECH 2008, Banff, AB, Canada, July 2008
- Searle SS (1999) Ice tank tests of a highly skewed propeller and a conventional ice-class propeller in four quadrants. PhD thesis, Memorial University of Newfoundland
- Hagesteijn G, Brouwer J, Bosman R (2012) Development of a six-component blade load measurement test setup for propeller-ice impact. In: 31st International conference on ocean, offshore and Arctic engineering (ASME 2012). American Society of Mechanical Engineers, pp 607–616
- Walker DLN (1996) The influence of blockage and cavitation on the hydrodynamic performance of ice class propellers in blocked flow. PhD thesis, Memorial University of Newfoundland
- Veitch B (1995) Predictions of ice contact forces on a marine screw propeller during the propeller-ice cutting process. In: *Acta Polytechnica Scandinavica, Mechanical Engineering Series*
- Veitch B, Bose N, Meade C, Liu P (1997) Predictions of hydrodynamic and ice contact loads on ice-class screw propellers. In: 16th International Conference on Offshore Mechanics and Arctic Engineering, Yokohama, Japan. *Offshore Mechanics and Arctic Engineering*
- Bose N, Veitch B, Doucet M (1998) A design approach for ice class propellers. *Trans Soc Naval Architects Mar Eng* 106:185–211
- International Association of Classification Societies (IACS) (2011) Requirements concerning the POLAR CLASS, I3: Machinery Requirements for Polar Class Ships. IACS Requirements 2006/Rev.1, 2007. International Association of Classification Societies (IACS)
- American Bureau Shipping (ABS) (2016) Part 6: optional systems and items, section 3: machinery requirements for polar class vessels. Rules for building and classing—steel vessels. American Bureau Shipping (ABS), Houston, TX, USA, January 2016 edition, pp 55–60
- Batrak YA, Serdjuchenko AM, Tarasenko AI (2013) Calculation of torsional vibration responses in propulsion shafting system caused by ice impacts. In: *Torsional Vibration Symposium*, Salzburg, Austria
- Barro RD, Lee D-C (2011) Excitation response estimation of polar class vessel propulsion shafting system. *Trans Korean Soc Noise Vib Eng* 21(12):1166–1176
- Polic D, Æsøy V, Ehlers S (2016) Transient simulation of the propulsion machinery system operating in ice—modeling approach. *Ocean Eng* 124:437–449
- Batrak Y, Serdjuchenko NM, Tarasenko A (2012) Calculation of propulsion shafting transient torsional vibration induced by ice impacts on the propeller blades. In: *Proceedings of world maritime technology conference*, Saint-Petersburg, Russia, May 29–June 1 2012. World Maritime Technology Conference
- Walker ND (2004) *Torsional vibration of turbomachinery*. McGraw-Hill, New York. ISBN 0071439377
- Nestorides EJ (1958) *A handbook on torsional vibration*. Cambridge University Press, London, UK
- Wu JS, Chen CH (2001) Torsional vibration analysis of gear-branched systems by finite element method. *J Sound Vib* 240(1):159–182
- Archer S (1955) Torsional vibration damping coefficients for marine propellers. *Eng* 1955:594–598
- Carlton JS (2012) Chapter 11: Propeller-ship interaction, 3rd edn. Elsevier Butterworth-Heinemann, Amsterdam, pp 265–278. ISBN 0080971237
- De Silva CW (2000) *Vibration : fundamentals and practice*, 2nd edn. CRC Press, Boca Raton. ISBN 0849319870
- Cai C, Zheng H, Khan M, Hung K (2002) Modeling of material damping properties in ANSYS. In: *CADFEM Users Meeting & ANSYS conference*, pp 9–11
- Burella G, Moro L (2017) Transient torsional analysis of polar class vessel shafting systems using a lumped model and finite element analysis. In: *The proceedings of The twenty-seventh (2017) international ocean and polar engineering conference*, San Francisco, California, pp 281–288, June 26–30 2017. ISOPE. ISBN 978-1-880653-97-5